Available online at www.sciencedirect.com
ScienceDirect
Journal of the European Ceramic Society 27 (2007) 357–366
www.elsevier.com/locate/jeurceramsoc

Synthesis of SiCNAl(O) pre-alloyed nanopowders by pyrolysis of an aluminosilazane aerosol

Vincent Salles *, Sylvie Foucaud, Etienne Laborde, Eric Champion, Paul Goursat

SPCTS, UMR CNRS 6638, Faculté des Sciences, 123 Avenue Albert Thomas, 87060 LIMOGES, France

Received 14 January 2006; received in revised form 14 April 2006; accepted 21 April 2006
Available online 30 June 2006

Abstract

A liquid aluminosilazane precursor, with various Al contents, was synthesized by direct reaction between hexamethyldisilazane and trimethylaluminum at room temperature. Mass spectrometry and Fourier-transform infrared spectroscopy showed respectively a methane evolution and the formation of Al–N bonds. Thermal-spray pyrolysis of this precursor was realized under different conditions: temperature (1200–1400 °C), pyrolysis atmosphere (Ar, Ar/NH_3) and gaseous flow rate (1 and 3 L min^{-1}). SEM micrographs revealed spherical SiCNAl(O) nanopowders which size (20–180 nm in diameter) depending on the residence time duration of the product in the furnace. Pyrolysis under argon led to a high C content, and then to the presence of free carbon and amorphous SiC phase detected by XRD and NMR analysis. Introduction of ammonia in the pyrolysis atmosphere induced an important decrease of C content in the pre-alloyed nanopowders, correlated with an increase of N and Al. With this process, multielement nanopowders with an adjustable composition exhibit a higher thermal stability than powders processed by laser-spray pyrolysis with an equivalent precursor.

Keywords: Powders-chemical preparation; Nanocomposites; SiCNAl powders; Structural applications

1. Introduction

Processing of dense silicon nitride-based materials, or Si_3N_4/SiC composites, needs sintering aids introduction, which often induces microstructural heterogeneities.[1–4] To overcome this phenomenon, different ways were explored mainly from organometallic precursors. Although this route led to excellent thermomechanical properties for SiC fibers,[5] its use does not give satisfying results for monolithic materials. Some experiments concerned also the sintering of powder blends and pre-pyrolysed powders, from polycarbosilane or polysilazane decomposition, in order to bind grains chemically. But whatever the process used, material properties are still low owing to the presence of cracks, porosity or segregated free carbon resulting from the release of gaseous species during thermal treatment.[6]

For all these reasons, a new route to produce dense silicon nitride-based materials, from nanopowder synthesis followed by a sintering step, seems to be more promising. The best interest of this approach is to favour an atomic scale distribution of sintering aids which should lead to an homogeneous microstructure after densification. One of the conventional methods is powder mixing in liquid media but it involves the use of dispersing agents and Si_3N_4-based powders do not have equivalent surface groups as oxides such as Al_2O_3 and Y_2O_3. Therefore, powder blends stabilization and final material homogeneity are very difficult to obtain.[7] On an other hand, nanostructured materials can be fabricated if an ultrafine multielement powder method is used. Several teams have worked and are still working on this route,[8–13] mainly using the laser-pyrolysis process, but their investigations concern mixtures of non-miscible precursors. They did not realize an unique hybrid precursor containing metallic elements needed for sintering.

The first papers about the fixation of boron or aluminum on silazanes,[14–18] to obtain directly monolithic ceramics after pyrolysis, have been published in the last two decades. From these results, we have undertaken the synthesis of hybrid precursors with a suitable viscosity for aerosol formation. Then, we have investigated their thermal decomposition in order to produce pre-alloyed nanopowders containing Si/C/N/Al/(O) elements.

* Corresponding author. Tel.: +33 5 55 45 74 61; fax: +33 5 55 45 75 86.
E-mail address: vincent.salles@unilim.fr (V. Salles).

0955-2219/$ – see front matter © 2006 Elsevier Ltd. All rights reserved.
doi:10.1016/j.jeurceramsoc.2006.04.168

2. Experimental details

2.1. Precursor synthesis

The monomer chosen for this study was a commercial hexamethyldisilazane (HMDS = $(Si(CH_3)_3)_2NH$, Aldrich). The aluminum compound used was trimethylaluminum (TMA = $(CH_3)_3Al$, Aldrich), in a 2 mol L^{-1} solution in hexane, which is very reactive and pyrophoric. So, it needed precautions for use. Handling and reactions were carried out under controlled atmosphere of argon (99.999 purity).

The precursor synthesis stemmed from a previous specific experimentation.[19] In this work, only experimental details related to the reaction between HMDS and TMA are presented. HMDS, kept into a glove box under argon, was transferred in the reaction flask and stirred vigorously. Then, TMA was slowly added at room temperature via a syringe. After the addition of TMA, the solution was stirred for 15 h at 20 °C. Finally, hexane was separated from hybrid precursor by distillation at 46 °C, under a partial vacuum of 100 mbar for 1 h. Different Al contents were studied, corresponding to Si/Al molar ratios: 5, 10, 15 and 30.

The reaction product (aluminosilazane) characterizations were performed with mass spectrometry (TA instrument SDT 2960, 1–55 UMA) and Fourier Transform IR (Spectrum One FT-IR, Perkin-Elmer). FT-IR analyses were carried out in absorbance mode (4000–400 cm^{-1}). All the samples were prepared in a glove box. A drop of silazane drop was deposited between two KBr windows, and the cell protected from ambient air pollution by a tight film.

2.2. Powder synthesis

Thermal conversion of the aluminosilazane into ceramic particles was performed in a thermal pyrolysis equipment. After removal of water vapor traces from the reactor by a preliminary vacuum pumping, the furnace was progressively heated up to the desired pyrolysis temperature. The liquid precursor was directly introduced in an aerosol generator device (RBI, Meylan, France) which frequency and power alimentations were adjusted to obtain the aerosol with a suitable yield, respectively around 800 kHz and 100 W. Briefly, the piezoelectric ceramic (made up of barium titanate) generates a beam of ultrasounds which, when its focused near the free surface of the liquid, forms a "fountain" and finally the aerosol. The sizes of droplets are constant, depending on liquid characteristics and ultrasound frequency. In this study, the aerosol temperature was held at 30 °C by a regulated water circulation to favour the reproductibility of all experiments.

An argon flow was used to carry the fine droplets towards the pyrolysis furnace, equipped with an alumina tube. During pyrolysis, the total pressure was fixed to 1000 mbar. The as-formed particles were finally trapped in two collectors containing filter-barriers made of microporous alumina (pore size #1 μm). The gaseous species were evacuated by a vacuum pumping system, and via a liquid nitrogen trap. Pyrolysis conditions were studied through three parameters: carrier gas flow rate (1 and 3 L min^{-1}), furnace temperature (1200–1400 °C) and atmosphere composition (Ar, Ar/NH_3). The aim was to obtain fine powders with high thermal stability and a versatile composition. All the powders were stored into a glove box under argon.

Different analytical techniques were used for the characterization: SEM observations (Philips XL 30, powders were scattered in an ethanol solution, using a drop of the suspension for observation after solvent evaporation), specific surface area measurements (Micromeritics: ASAP 2010, BET 8 pts, N_2), X-ray diffraction measurements (Siemens, D5000, 2θ, Cu $K\alpha_1$), FT-IR spectroscopy (Spectrum One FT-IR, Perkin-Elmer, using KBr pellets method), ^{29}Si NMR, ^{27}Al NMR and ^{13}C NMR spectroscopy (Brücker spectrometer, 400 MHz/89 mm, Service de RMN du solide, GDPC, Université de Montpellier II), and elemental analysis (Service central d'Analyse du CNRS, Vernaison, France). Several analytical techniques were used: Si and Al by ICP-AES technique after chemical dissolution, C by combustion to 1800 °C under oxygen, and N by pyrolysis to 3000 °C under He in a graphite crucible.

3. Results and discussion

3.1. Precursor synthesis

TMA introduction into HMDS, at room temperature, led to a visible gas evolution as soon as the first droplets had been added. The gas reaction products analysed by mass spectrometry (Fig. 1) showed species corresponding to 15 and 16 *m/z*. It has been shown that the release of ammonia during heat treatment of silazanes starts only above 90–100 °C.[20] Consequently, $m/z = 16$ and 15 seem to correspond to methane evolution and to a by-product CH_3^+ formed in the quadrupole. Moreover, taking into account the molecular structure of the starting compounds, the methane formation should result from a reaction between the N–H and Si–CH_3 groups. At the very beginning, the reaction kinetic is fast, but then, the gas evolution decreases slowly. This explains our choice for a 15 h stirring duration to make sure the reaction was achieved.

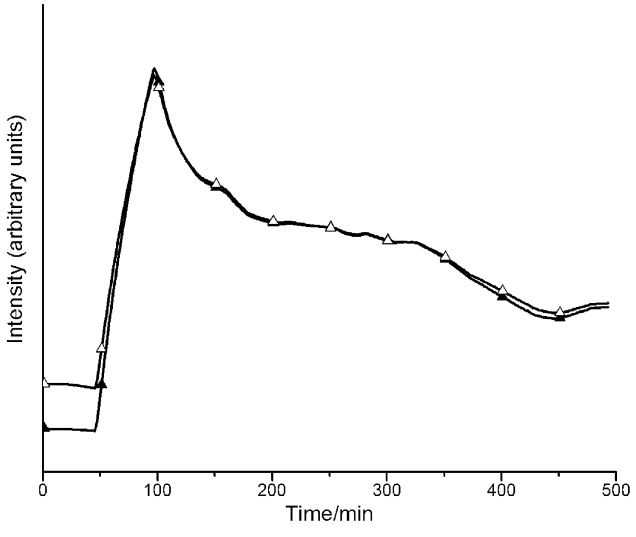

Fig. 1. Mass spectrometry of gaseous species: $m/z = 15$ (▲) and $m/z = 16$ (△).

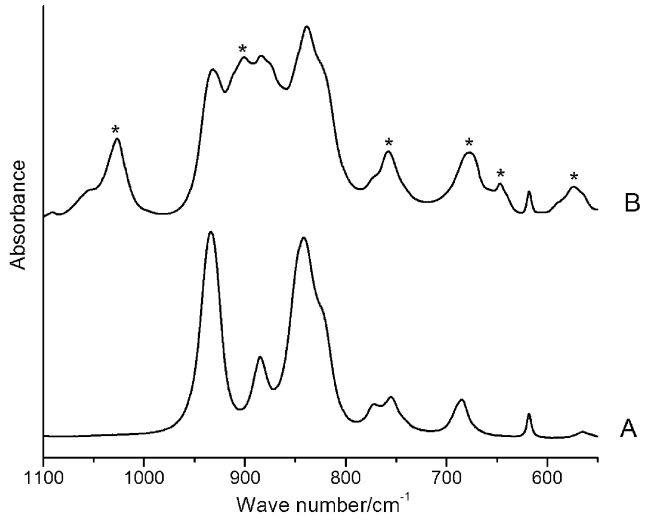

Fig. 2. FT-IR spectra of HMDS (A) and the aluminosilazane (B) (1100–550 cm^{-1}); *Al—N bond.

FT-IR spectra for pure HMDS and HMDS after reaction with TMA are shown in Fig. 2 for Si/Al = 30. The product spectrum contains new bands (indexed in Table 1) that could be assigned to a Al–N bond formation. The reaction with TMA induces a decrease of the N–H band (1181 cm^{-1}) which implies that N–H is the silazane reactive group. On the other hand, the similar intensity measured for C–H (2955 cm^{-1}) on both spectra (Fig. 3) illustrates that the presence of methyl groups remains important, and shows that only a part of Al–CH_3 of TMA had reacted with the N–H bonds of HMDS. A three-nitrogened aluminum formation seems to be unlikely, may be due to an important steric hindrance.

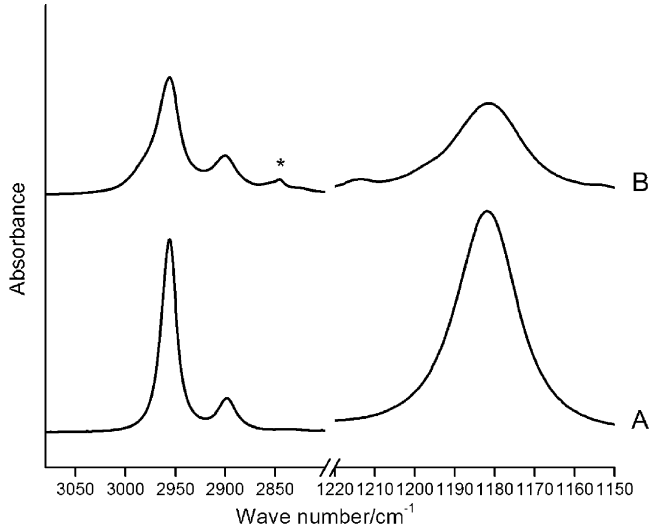

Fig. 3. FT-IR spectra of HMDS (A) and the aluminosilazane (B) (3100–2800 and 1220–1150 cm^{-1}); *Al—N bond.

Table 1
FT-IR wave number values for pure HMDS and corresponding new bands after reaction with TMA

Wave number (cm^{-1})		Vibration mode
Pure HMDS	New bands (after reaction)	
3382	–	N–H stretching[21–24]
2955	–	C–H asym. stretching[21–23,25]
2896	–	C–H sym. stretching[21–23,25]
	2850	C–H stretching in Al–CH_3[26,27]
1440	–	–CH_3 in Si–CH_3 asym. deformation[21]
1401	–	
1253	–	C–H in Si–CH_3 sym. deformation[21,23–24]
	1205	C–H stretching in Al–CH_3[26,27]
1181	–	N–H bending[21,24,28–29]
	1026	Al–N[30]
933	–	Si–N–Si asym. stretching[22–24,28]
	900	Al–N[31]
884	–	Si–H bending[21–23]
841	–	–CH_3 rocking in $SiCH_3$[21,23–24]
772	–	Si–C in Si–CH_3 asym. stretching[21–22]
	758	Al–N stretching[21,31–36]
755	–	Si–C in Si–CH_3 sym. stretching[21–22,35]
	689	Al–N[35–40]
684	–	Si–C asym. stretching[28]
	647	Al–N[21,31–33]
618	–	Si–C stretching[21]
	574	Al–N[30,32,40]

These results prove that aluminum can be fixed on a silazane monomer by direct reaction at room temperature between HMDS and TMA, with a methane evolution according to reaction (1).

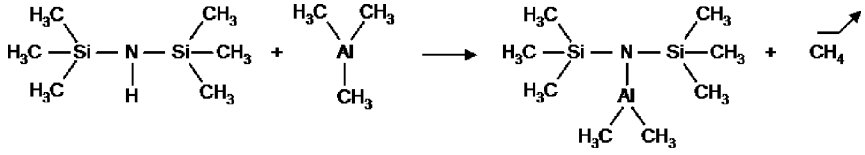

(1)

In addition to previous investigations devoted to the synthesis of solid polyaluminosilazanes from reaction between tetramethyldisilazane (or similar silazanes) and TMA (or triethylaluminum, or dimethylaluminum amide), this study shows that colorless liquid aluminosilazanes can be prepared with Si/Al ratios higher than 5.[18] The effect of Al content is visible in so far as the apparent viscosity increases with the quantity of Al in the precursor. This phenomenon could be explained by an increase of aluminosilazane molecular mass and/or of interactions between molecules which could form a linked-liquid. Due to its high hydrolysis sensitivity, the colorless liquid becomes a white solid as soon as the atmosphere contains traces of water vapor.

3.2. Powder synthesis

For clarity of the presentation, a particular nomenclature is used to identify each powder batch (Table 2) that gives an account of pyrolysis conditions (temperature, atmosphere, gaseous flow rate) and Si/Al ratio.

Table 2
Pyrolysis conditions and nomenclature

Powder batches	Initial Si/Al molar ratio	Pyrolysis temperature (°C)	Atmosphere	Total flow rate (L min^{-1})
12A1L30	30	1200	Ar	1
12A3L30				3
13A1L30		1300		1
13A3L30				3
14A1L30		1400		1
14A3L30				3
14A3L15	15	1400	Ar	3
14A3L10	10			
14A3L05	5			
14AN3L15	15		Ar/NH_3 (75/25, v/v)	3

Table 3
Specific surface area and particle size

Batches	Specific surface area (m^2 g^{-1})	Equivalent disc diameter (nm)[a]
12A1L30	18	139
12A3L30	32	78
13A1L30	19	132
13A3L30	37	68
14A1L30	20	132
14A3L30	32	78

[a] d_{eq} (nm) = 6000/($d_{th.}$ S_{BET}); with d_{th} = 2.4 and S_{BET} expressed in m^2 g^{-1}.

3.2.1. Influence of pyrolysis temperature and carrier gas flow rate

On SEM micrographs (Fig. 4), spherical grains with a rather narrow granulometric distribution are observed. In the studied temperature range, the particle size seems to be unchanged whatever the decomposition temperature of the precursor might be. Contrary to the temperature, the flow rate variation implies a change of the particle size. The more the flow rate increases the smaller the particles are. In the furnace, the precursor decomposition leads to the formation of gaseous species, and then to solid particles by recombination these radicals. In these conditions, the growth process of the particles is controlled by the residence time of the gaseous species in the reactional zone. Thus, this phenomenon is related to the carrier gas flow rate.

These changes are confirmed by the specific surface area and the values of equivalent disc diameter calculated with a density of 2.4 measured by helium pycnometry (Table 3). These as-fabricated powders are dense since the calculated diameters are consistent with those of observed particles (Fig. 4). The powders synthesized by laser pyrolysis are slightly smaller than those obtained in this study for similar precursors and pyrolysis parameters. The finer particle size in the laser-driven process, 30–70 nm (49–26 m^2 g^{-1}),[10] is due to a shorter residence time in the reactional zone than in the case of thermal pyrolysis. The temperature gradients considered are 10^3–10^4 °C s^{-1} and 10^2 °C s^{-1}, respectively, and the length of the furnace isotherm zone is about ten times higher than the laser one.

Table 4 presents the elemental compositions of powders synthesized at 1200, 1300 and 1400 °C, as well as theoric (initial mixture) and final (measured) C/N, C/Si, Si/N and Si/Al ratios. Whatever the pyrolysis conditions, C appears to be the major species, with a content value 2–3 times higher than Si and 4–6 times than N. Flow rate change, from 1 to 3 L min^{-1}, induces a decrease of carbon content of about 10 wt.%. Consequently, Si, N and Al contents logically increase. One can notices that changes of pyrolysis temperature, in the studied range, do not have a significant effect on powder composition.

This flow rate effect is clearly shown by C/N and C/Si ratios which are reduced to 30% with an increase from 1 to 3 L min^{-1}. Resulting from silazane decomposition, carbon contained species are faster evacuated which limits their recombination in solid particles. This is confirmed by laser pyrolysis results, with a shorter residence time in the reactional zone, carbon contents are lower for the conversion of HMDS under argon.[41]

Si/N values are similar (2.1–2.2) at 1300–1400 °C and whatever flow rate conditions, but they are slightly higher than theoric ones (2.0). This can be explained by a decrease in nitrogen content due to transamination reactions that involve ammonia evolution during precursor heating.[42] Nevertheless, this loss is less significant than compositional changes induced by carbon content variations.

The final Si/Al ratios are clearly superior to the theorical one, but Al content is twice higher when the flow rate increases from 1 to 3 L min^{-1}. Thus, the carrier gas velocity has an important effect on the final powder composition. Its variation involves a residence time modification of the precursor in the pyrolysis furnace.

Table 4
Chemical composition of nanopowders

Batches	Composition (wt.%)				Molar ratio							
	Si	C	N	Al	C/N		C/Si		Si/N		Si/Al	
					Th.[a]	Final	Th.[a]	Final	Th.[a]	Final	Th.[a]	Final
12A1L30	40.3	52.2	11.6	0.3	6.2	5.3	3.1	3.0	2.0	1.7	30.0	129.1
12A3L30	47.5	34.8	15.2	0.5		2.7		1.7		1.6		91.3
13A1L30	38.4	48.5	8.7	0.1		6.4		3.0		2.2		615.2
13A3L30	48.2	38.7	10.7	0.2		4.2		1.9		2.2		308.6
14A1L30	37.6	49.7	8.7	0.2		6.6		3.1		2.1		212.5
14A3L30	46.0	40.8	10.7	0.4		4.4		2.1		2.1		100.5

[a] Calculated from quantities of reactants used for the aluminosilazane synthesis.

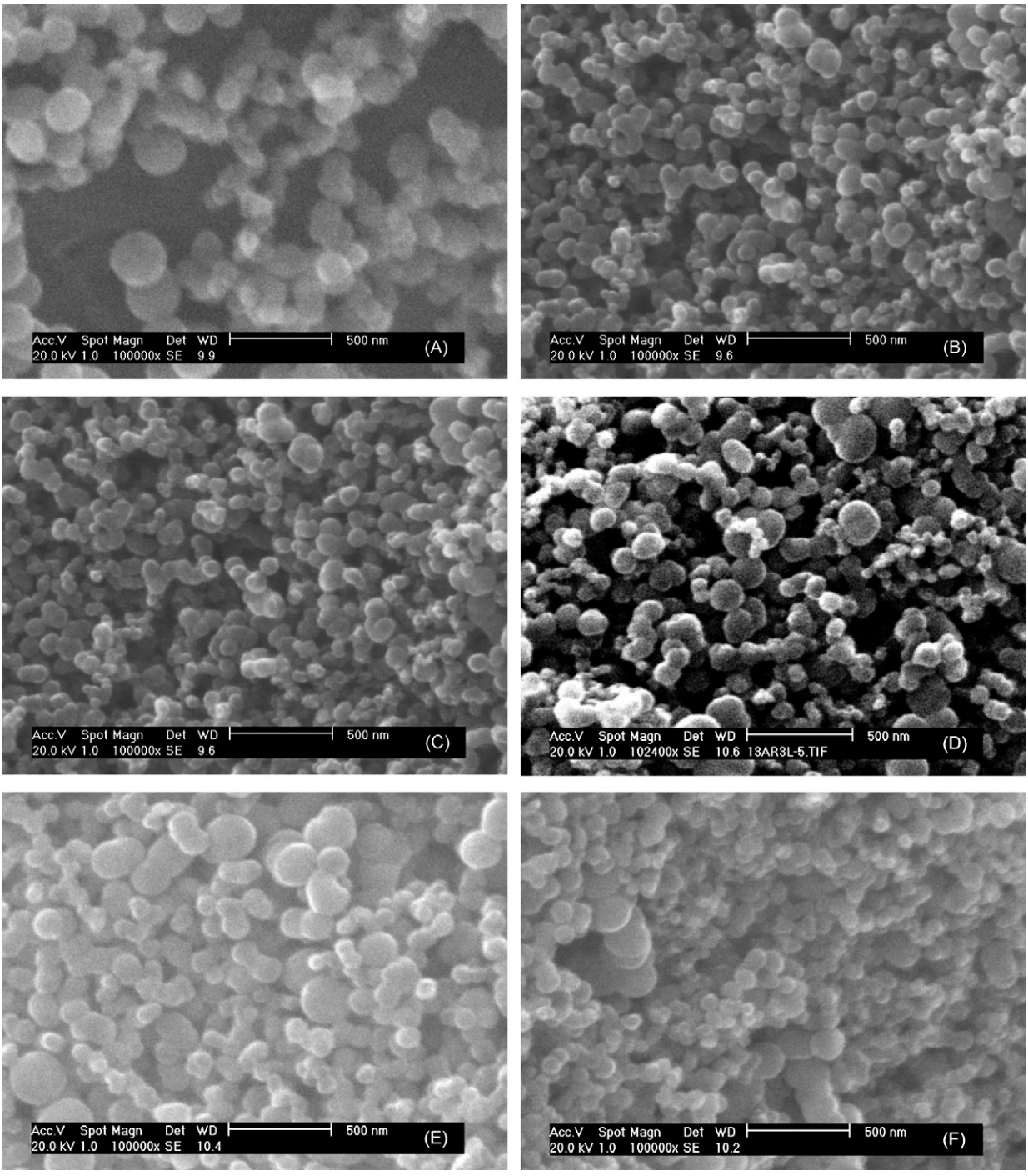

Fig. 4. SEM micrographs of powders synthesized at 1200–1400 °C, with a 1–3 L min^{-1} flow rate: 12A1L30 (A), 12A3L30 (B), 13A1L30 (C), 13A3L30 (D), 14A1L30 (E) and 14A3L30 (F).

X-ray diffractograms (Fig. 5) show the formation of an amorphous structure after pyrolysis for all powder batches, but a structural rearrangement seems to progress with the decomposition temperature of the precursor. This phenomenon is emphasized by the formation of two pics around $2\theta = 26°$ and 35°, which correspond to graphite carbon and β-SiC respectively.[43] A part of the batch 14A1L30 was heat treated up to 1400 °C, for 5 h under nitrogen atmosphere. The resulting powder still presents a partial amorphous character indicating a slow crystallization rate (Fig. 5, 14A1L30-1400-5h), but a great thermal stability, which is confirmed by the TG analysis (Fig. 6).

Compared to a powder synthesized from HMDS aerosol with a laser pyrolysis process under argon atmosphere,[41] the powder synthesized from thermal pyrolysis appears to be more stable since its weight gain is very low while the mass loss of the laser powder is near 3 wt.% at 1400 °C. The TG analysis of this powder was carried out under a N_2/He (20/80) mixture, but the authors showed that the amount of helium did not influence the

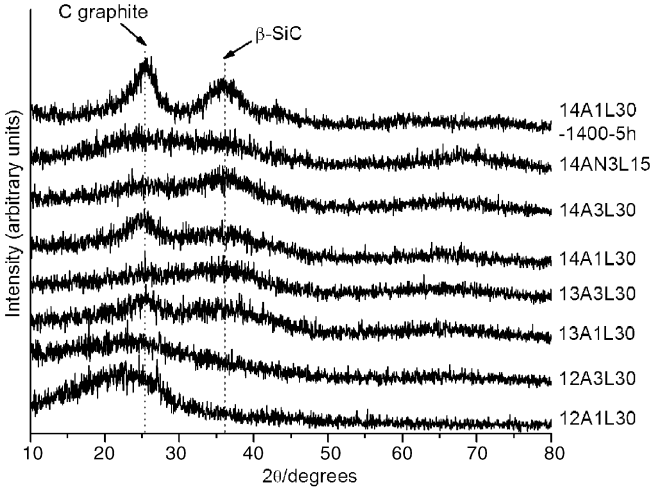

Fig. 5. XRD patterns of powders synthesized under different pyrolysis conditions.

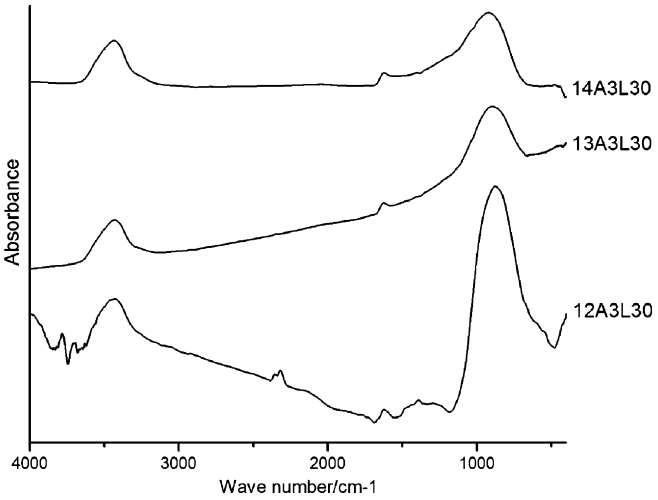

Fig. 7. FT-IR spectra of powders synthesized at 1200–1400 °C.

thermal stability up to 1500 °C. For this technique, the thermal stability of the powder can be increased using gaseous reactant species like SiH_4, CH_3NH_2 and NH_3, but this process is quite hazardous and more expensive.[12] Moreover, the in situ introduction of gaseous precursors of heteroelements (like Al) in the synthesized powders was not demonstrated, maybe due to the high difficulty to handle the precursors, and to the complexity of the reactions induced. To explain the differences between these two methods, the residence time and the cooling rate can be mentioned, as it was previously seen for the particle size. The advancement of the precursor conversion is promoted when using the furnace device.

FT-IR spectra (Fig. 7) of the powders exhibit the same bands whatever the flow rate of carrier gas and the precursor pyrolysis temperature may be. A broad band from 700 to 1100 cm^{-1} centered on 900 cm^{-1}, can be assigned to Si–N–Si and Si–C bonds in an amorphous SiCN structure (Table 1).[10,44] It characterizes a low structural organization degree in agreement with DRX diagrams (Fig. 5). Absorption bands situated at 1631 and 3424 cm^{-1} are assigned to O–H bond vibrations, certainly arising from water adsorbed on the powder surface during sampling and analysis in air. This water detection is usually observed in FT-IR spectra of fine particles since the technique only allows a surface analysis of the specimens.

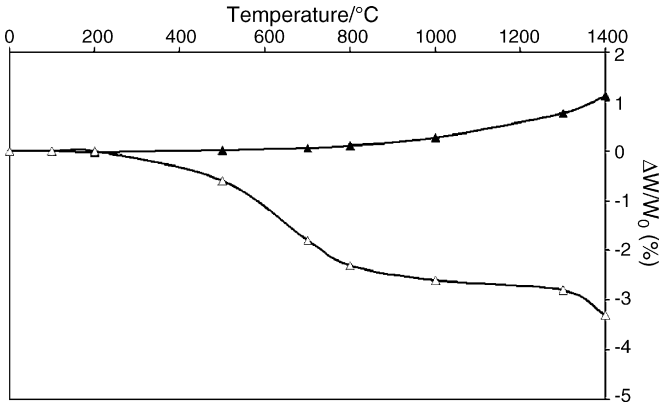

Fig. 6. TG profiles of 14A1L30 (▲) and HMDS0 (△) (synthesized by laser-pyrolysis of HMDS under Ar), under pure N_2 and N_2/He (20/80) mixture flows, respectively.

^{29}Si NMR and ^{13}C NMR spectra for 13A1L30, 14A1L30, 13A3L30 and 14A3L30 are shown in Fig. 8, respectively on (a), (b), (c) and (d) spectra. All ^{29}Si spectra (Fig. 8(1)) contain a broad peak centered at −20 ppm, linked to environments such as SiC_4 and/or SiC_2N_2.[45] Other peaks at −35, −45 ppm and 4 ppm, corresponding respectively to SiN_4, $SiCN_3$ and SiC_3N, have a low intensity in these spectra. It means that silicon has a carbon rich environment, but this result is not surprising in view of the high carbon content in the powders detected by elemental analysis. The Si–C bond presence is confirmed by ^{13}C spectra (Fig. 8(2)) with a peak centered at 30 ppm (CSi_4). A second one at 130 ppm, of a greater intensity, indicates the presence of free carbon (sp^2) in the as-formed powders.

Contrary to the flow rate of carrier gas, the pyrolysis temperature does not influence the final composition and morphology of the powders. This parameter was fixed on 1400 °C for further experiments to favour the precursor decomposition and thus improve the powder thermal stability. Concerning the carrier gas, the higher rate of argon (3 L min^{-1}) seems to be the more interesting because it limits the residence time in the reactional zone, with a decrease of the particle size, a higher C loss during pyrolysis and the formation of powders more rich in Si, N and Al.

3.2.2. *Influence of the Al content in the precursor*

Aluminum content of the powders presented (Section 3.2.1) remains too low (Si/Al = 100) compared to the alumina content necessary to process dense materials. Previous works dealing with Si_3N_4 and Si_3N_4/SiC sintering showed that the optimum conditions are obtained with a liquid phase resulting from the addition of 6 wt.% of Y_2O_3 and 3 wt.% of Al_2O_3.[46] This powder composition corresponds to a molar ratio Si/Al = 50. In order to fabricate powders with various Al contents, for a further study of sintering behaviour, we have pyrolysed different aluminosilazanes with Si/Al molar ratios of 15, 10 and 5.

Table 5
Chemical composition of nanopowders

Batches	Composition (wt.%)				Molar ratio							
	Si	C	N	Al	C/N		C/Si		Si/N		Si/Al	
					Th.	Final	Th.	Final	Th.	Final	Th.	Final
14A3L30	46.0	40.8	10.7	0.4	6.2	4.4	3.1	2.1	2.0	2.1	30.0	100.5
14A3L15	36.6	45.8	11.9	0.5	6.4	4.5	3.2	2.9		1.5	15.0	74.9
14A3L10	36.9	43.3	13.2	0.7	6.6	3.8	3.3	2.7		1.4	10.0	53.7

The SEM micrographs of the corresponding synthesized powders reveal spherical particles with a constant specific surface area whatever the Si/Al ratio may be.

Elemental analyses (Table 5) realized on the different batches indicate that Al content in the aluminosilazane increases with decreasing of Si/Al ratios from 30 to 10. But this was not observed for lower values due to a too high viscosity of the precursor preventing its correct nebulization. With viscous aluminosilazane precursors, the temperature of the aerosol generator device must be higher than 30 °C to obtain good nebulization yields. Despite the increasing Al content, the final values remain around five times lower than the theoric ones. In view of the pyrolysis process, the most probable assumption is that the Al–N bond is less thermally stable than Si–C and Si–N. On the other hand, the Si/Al value for 14A3L10 is near 50 which corresponds to a 3 wt.% alumina content in silicon nitride, the ideal value for Si_3N_4 densification.[46]

NMR spectra (Fig. 9) are representative of all the powders. The ^{27}Al NMR spectra (Fig. 9(a)) have a similar shape, mainly composed of two broad peaks, centered at 100 and 0 ppm. Between these two values, there is a region with a non-negligible intensity certainly due to an overlap of the peaks, but the presence of an intermediate peak must be considered. The peak positions for the ^{27}Al spectra are not defined precisely as mentioned in the literature (Table 6). From previous results, the chemical shifts at 100 ppm can be assigned to $[AlN_4]$ environment, while the peak at 0 ppm may correspond to $[AlX_6]$ (X = O or N). Initial reagents are compounds free from oxygen, thus it can be supposed that Al elements are preferentially linked to nitrogen ones. But the presence of mixed environments as $[Al(O,N)_y]$ cannot be excluded, that may result from powder contamination by traces of oxygen.

The ^{29}Si NMR and ^{13}C NMR spectra (Fig. 9(b) and (c)) are consistent with the ^{27}Al ones because there is no difference detected between the batches studied. As shown in Section 3.2.1, ^{29}Si (Fig. 9(b)) spectra exhibit a broad peak centered at −20 ppm which characterizes $[SiC_4]$ and/or $[SiC_2N_2]$ environments, and a high carbon content is still present, with free C and CSi_4 visible in the ^{13}C spectra (Fig. 9(c)) at 130 and 30 ppm, respectively.

The final Si/Al ratios measured are equal to, or higher than 50, which corresponds to the optimum content for the densification of Si_3N_4 material, but for an accurate determination of Al environments, it is necessary to reach a higher percentage. Experiments are in progress.

Table 7
Chemical composition of nanopowders

Batches	Composition (wt.%)					Molar ratio			
	Si	C	N	Al	O	C/N	C/Si	Si/N	Si/Al
14A3L15	36.6	45.8	11.9	0.5	–	4.5	2.9	1.5	74.9
14AN3L15	45.5	3.4	46.6	0.9	5.1	0.1	0.2	0.5	49.1
HMDS0[a]	51	32	15	–	2	2.5	1.5	1.7	–
HMDS40[b]	51	6	38	–	5	0.2	0.3	0.7	–

[a] Laser pyrolysis of a pure HMDS aerosol in Ar atmosphere.[12]
[b] Laser pyrolysis of a pure HMDS aerosol in Ar/NH_3 (60/40, flow rate ratio) atmosphere.[12]

3.2.3. *Influence of the pyrolysis atmosphere*

It is well known that the presence of free carbon in Si_3N_4/SiC powders has a deleterious effect on the sintering behaviour. The efficiency of an ammonia addition in the pyrolysis atmosphere to reduce the final carbon content was shown in several previous investigations.[12,44,50] So ammonia was added to the carrier gas (NH_3/Ar = 25/75 vol.%) with a total flow rate of 3 L min^{-1} in the aerosol generator device, for a pyrolysis at 1400 °C of an aluminosilazane with a ratio Si/Al = 15. To discuss these results, the chemical compositions of powders issued from similar precursors pyrolysed under argon or Ar/NH_3 mixtures with two heating techniques are summarized in Table 7. A comparison of the chemical compositions shows an important decrease of

Table 6
Chemical shifts of Al environments in nitride, oxinitride and oxide compounds

Al environments, chemical shifts			Corresponding studies
Octahedral	Pentahedral	Tetrahedral	
AlN_6 (6 ppm)	AlN_5 (intermediate values, mainly 30–50 ppm)	AlN_4 (103 ppm)	Study of SiC/AlN systems[47]
AlO_6 (0 ppm)	AlO_5 (35 ppm)	Mixed $Al(O,N)_4$ tetrahedral sites (110–65 ppm); AlO_4 (60 ppm)	Si–Al–O–N glasses[48]
AlO_6 (14 ppm)	$[AlO_yN_{4-y}]$ (66–71 ppm)	AlN_4 (114–115 ppm)	Study of impurity phases in β-sialon ceramics[49]

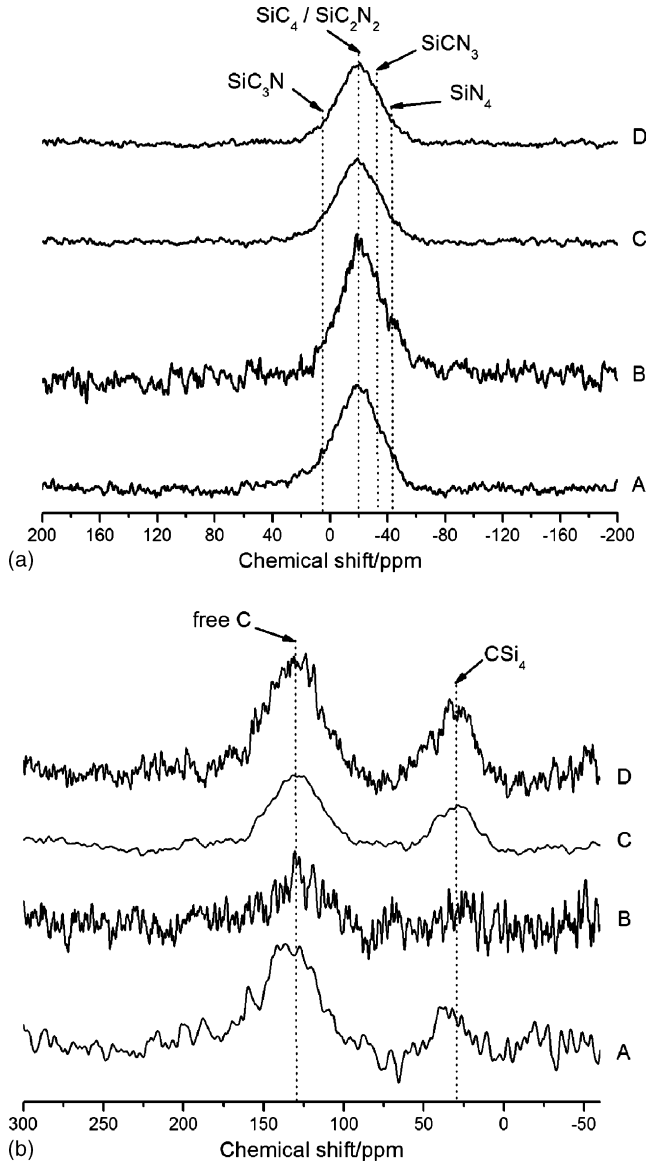

Fig. 8. ^{29}Si NMR (a) and ^{13}C NMR (b) spectra of 13A1L30 (A), 13A3L30 (B), 14A1L30 (C) and 14A3L30 (D) powders.

carbon content from 45.8 to 3.4 wt.% with a thermal pyrolysis process and from 32 to 6 wt.% with a laser process when ammonia is incorporated in the carrier gas. This carbon loss is equally displayed by the XRD diffractogram (Fig. 5) with a decrease of the β-SiC peak ($2\theta = 35^\circ$).

The final compositions of HMDS 40 and 14AN3L15 powders are in good agreement since carbon is the minor element whereas silicon and nitrogen contents are the highest. The nitridation induced by ammonia during the precursor conversion could be due to a nucleophilic displacement of carbon in the Si–CH_3 groups according to reaction (2).[50] Nevertheless, an addition of 25 wt.% of NH_3 in the thermal pyrolysis process induces a more important loss of carbon than 40 wt.% of NH_3 in the laser process. The best nitridation effect for the thermal pyrolysed powder could be explained by different pyrolysis mechanisms and certainly by the kinetics of these reactions. As indicated before (Section 3.2.1), the residence time in the reactional zone

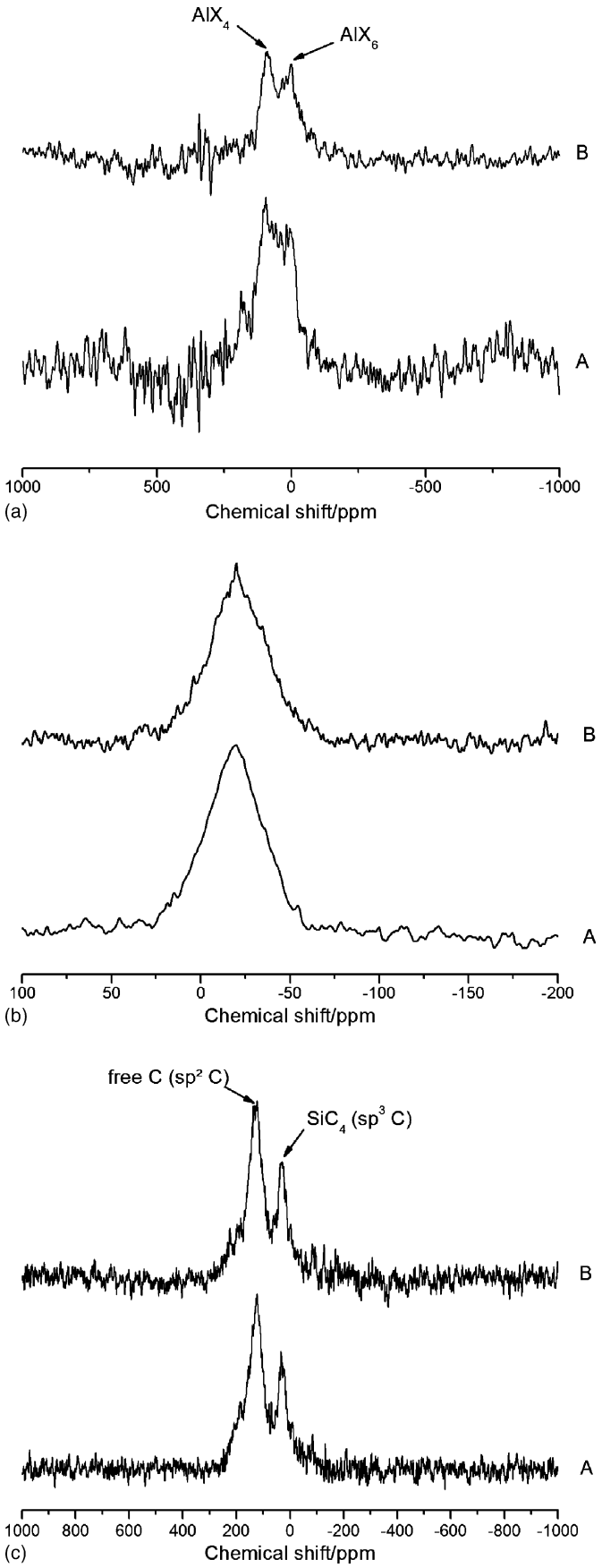

Fig. 9. ^{27}Al NMR (a), ^{29}Si NMR (b) and ^{13}C NMR (c) spectra for Si/Al = 15 (A) and 30 (B).

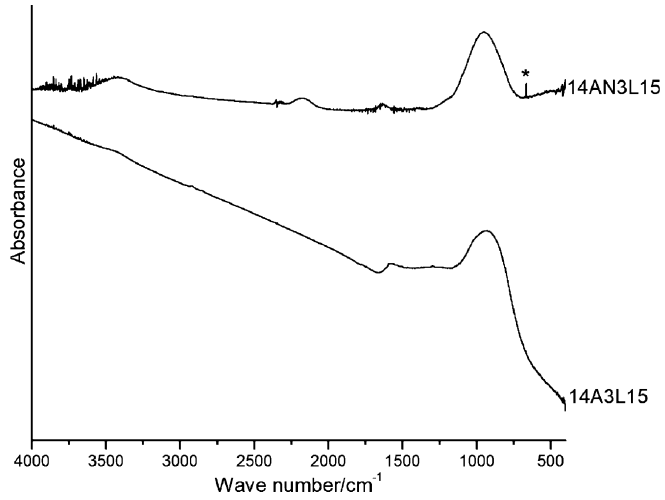

Fig. 10. FT-IR spectra of powders synthesized under pure Ar and NH_3/Ar mixture; *Al—N bond.

is shorter in the case of the laser process. Comparing the two powders considered in this study, the ammonia addition into the pyrolysis atmosphere induces an increase of Al content when the same precursor is used. A high temperature stabilization of the Al–N bonds, by nitriding species, seems to be the more probable assumption. Experiments are in progress to quantify this effect.

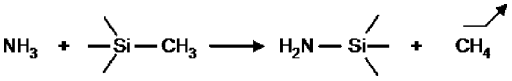

(2)

The oxygen detected (5 wt.%) certainly arises from water adsorption on the particles surface during sampling owing to their high specific surface area and their high nitrogen content.

This interpretation is confirmed by the powder IR spectrum in Fig. 10, presenting a broad band centered at 3400 cm^{-1} and a second one (with a lower intensity) at 1630 cm^{-1} which characterize O–H bond vibrations. The two powders exhibit a band centered on 950 cm^{-1}, corresponding to the Si–N–Si and Si–C bonds in a SiCN structure as seen in Section 3.2.1; a very small one at 660 cm^{-1} which could be assigned to the Al–N bond, in view of references in Table 1. It would be consistent with the elemental analyses since the Al content is twice higher in the powder synthesized in argon/ammonia mixture. A wide band, visible around 2180 cm^{-1}, is detected in this batch, and according to previous works this could correspond to the C≡N bond, which would be in agreement with the high N content in the powders.[51–53]

4. Conclusions

The high intrinsic mechanical properties of Si_3N_4/SiC materials are often restricted by the presence of microstructural defects, closely linked to the fabrication process (powder mixing of sintering aids, shaping, etc.) and to the starting grain size of the powders used. The improvement of these properties go through the synthesis of pre-alloyed nanopowders with suitable composition and thermal stability, but it necessitate hybrid precursors.

By reaction between HMDS and TMA at room temperature, it is possible to obtain a liquid aluminosilazane, with a versatile composition, for various Si/Al (5, 10, 15 and 30).

The combination of this new precursor and the thermal-spray pyrolysis process led to spherical SiCNAl(O) nanopowders. Their thermal stability appeared to be higher than that of powders synthesized by laser-driven process. Finally, the pyrolysis carried out under Ar/NH_3 atmosphere showed that the ideal Al content (equivalent to 3 wt.% of Al_2O_3 in Si_3N_4) could be reached by this method. The flexibility of the process allows that other heteroelements may be used for this SiCN-based systems.

Acknowledgements

The authors wish to thank P. Gaveau for the solid NMR analyses (GDPC, Université Montpelleir II, France) and D. Tétard for his contribution for the setting of the pyrolysis device (SPCTS, Université de Limoges, France).

References

1. Terwilliger, G. F. and Lange, F. F., Pressureless sintering of silicon nitride. *J. Mater. Sci.*, 1975, **10**, 1169–1174.
2. Greskovich, C., Prochazka, S. and Rosolowski, J. H., The sintering behaviour of covalently-bonded materials. In *Proceedings of the NATO Advanced Study Institute on Nitrogen Ceramics (No. 23)*, ed. F. L. Riley, 1977, pp. 351–357.
3. Mary, J.P., Lortholary, P., Goursat, P. and Billy, M., Densification de l'oxynitrure de silicium, French Patent, Fr 7,309,345 (1973).
4. Chartier, Th., Besson, J. L. and Goursat, P., Microstructure, oxidation and creep behaviour of β′-SiAlON ceramics. *Int. J. High Technol. Ceram.*, 1986, **2**, 33–45.
5. Yajima, S., Okamura, K., Hayashi, J. and Omori, M., Synthesis of continuous SiC fibres with high tensile strength. *J. Am. Ceram. Soc.*, 1976, **59**(7–8), 324–327.
6. Riedel, R., Passing, G., Schöfelder, H. and Brook, R. J., Synthesis of dense silicon-based ceramics at low temperatures. *Nature*, 1992, **355**, 714.
7. Mayne, M., Elaboration, microstructure et comportement au fluage de nanocomposites Si_3N_4/SiC. PhD Thesis, Université de Limoges, France, 1997.
8. Borsella, E., Botti, S., Fantoni, R., Alexandrescu, R., Morjan, I., Popescu, C. *et al.*, Nanocomposite ceramic powder production by laser-induced gas-phase reactions. *J. Mater. Res.*, 1992, **7**, 2257.
9. Haggerty, J. S. and Cannon, R. W., *Laser-induced Chemical Processes, Sinterable Powders from Laser-driven Reactions*. Plenum Press, New York, 1981, pp. 165–241.
10. Cauchetier, M., Croix, O., Luce, M., Baraton, M. J., Merle, T. and Quintard, P., Nanometric Si/C/N powders: Laser synthesis and IR characterization. *J. Eur. Ceram. Soc.*, 1991, **8**, 215–219.
11. Cauchetier, M., Armand, X., Herlin, N., Mayne, M., Fusil, S. and Lefevre, E., Si/C/N nanocomposirte powders with Al (and Y) additives obtained by laser spray pyrolysis of organometallic compounds. *J. Mater. Sci.*, 1999, **34**, 5257–5264.
12. Bahloul-Hourlier, D., Doucey, B., Laborde, E. and Goursat, P., Investigations on thermal reactivity of Si/C/N nanopowders produced by laser aerosol or gas interactions. *J. Mater. Chem.*, 2001, **11**, 2028–2034.
13. Mayne, M., Bahloul-Hourlier, D., Doucey, B., Goursat, P., Cauchetier, M. and Herlin, N., Thermal behaviour of SiCN nanopowders issued from laser pyrolysis. *J. Eur. Ceram. Soc.*, 1998, **18**, 1187–1194.
14. Seyferth, D. and Plenio, H., Borasilazane polymeric precursors for borosilicon nitride. *J. Am. Ceram. Soc.*, 1990, **73**, 2131–2133.
15. Soraru, G. D., Ravagni, A. and Campostrini, R., Synthesis and characterization of beta'-SiAlON ceramics from organosilicon polymers. *J. Am. Ceram. Soc.*, 1991, **74**, 2220–2223.

16. Funayama, O., Kato, T., Tashiro, Y. and Isoda, T., Synthesis of a polyborosilazane and its conversion into inorganic compounds. *J. Am. Ceram. Soc.*, 1993, **76**, 717–723.
17. Iwamoto, Y., Kikuta, K.-I. and Hirano, S.-i., Microstructural development of Si_3N_4-SiC-Y_2O_3 ceramics derived from polymeric precursors. *J. Mater. Res.*, 1998, **13**, 353–361.
18. Boury, B. and Seyferth, D., Preparation of Si/C/Al/N ceramics by pyrolysis of polyaluminasilazanes. *Appl. Org. Chem.*, 1999, **13**, 431–440.
19. Salles, V., Foucaud-Raynaud, S., Granet, R., Besson, J.-L. and Goursat, P., Synthèse de précurseurs polyaluminosilazanes. In *Proceedings of the Groupe Français de la Céramique*, 2004, p. 111.
20. Choong Kwet Yive, N.S., Polysilazanes fonctionnels—Précurseurs de carbonitrure de silicium. PhD Thesis, Université de Montpellier II, 1990.
21. Anderson, D. R., Infrared, Raman and ultraviolet spectroscopy. In *Analysis of Silicones*, ed. A. L. Smith. Wiley, New York, 1974, pp. 247–286.
22. Yu, G.-E., Edirisinghe, M. J., Finch, D. S., Ralph, B. and Parrick, J., Synthesis of alpha-silicon nitride powder from a polymeric precursor. *J. Eur. Ceram. Soc.*, 1995, **15**, 581–590.
23. Kim, M. T. and Lee, J., Characterization of amorphous SiC:H films deposited from hexamethyldisilazane. *Thin Solid Films*, 1997, **303**, 173–179.
24. Li, Y., Zheng, Z., Reng, C., Zhang, Z., Gao, W., Yang, S. *et al.*, Preparation of Si–C–N–Fe magnetic ceramics from iron-containing polysilazane. *Appl. Org. Chem.*, 2003, **17**, 120–126.
25. Li, Y.-L., Kroke, E., Riedel, R., Fasel, C., Gervais, C. and Babonneau, F., Thermal cross-linking and pyrolytic conversion of poly(ureamethylvinyl)silazanes to silicon-based ceramics. *Appl. Org. Chem.*, 2001, **15**, 820–832.
26. Lakomaa, E.-L., Root, A. and Suntola, T., Surface reactions in Al_2O_3 growth from trimethylaluminium and water by atomic layer epitaxy. *Appl. Surf. Sci.*, 1996, **107**, 107–115.
27. Uusialo, A.-M., Pakanen, T. T., Kröger-Laukkanen, M., Niinistö, L., Hakala, K., Paavola, S. *et al.*, Heterogenization of racemic ethylenebis(1-indenyl)zirconium dichloride on trimethylaluminum vapor modified silica surface. *J. Mol. Catal. A: Chem.*, 2000, **160**, 343–356.
28. Bao, X. and Edirisinghe, M. J., Polycyclodisilazane: a new polymeric precursor for silicon nitride-based ceramics. *J. Mater. Chem.*, 2000, **10**, 395–401.
29. Trabl, S., Suttor, D., Motz, G., Rössler, E. and Ziegler, G., Structural characterisation of silicon carbonitride ceramics derived from polymeric precursors. *J. Eur. Ceram. Soc.*, 2000, **20**, 215–225.
30. Raveh, A., Weiss, M., Pinkas, M., Rozen, D. Z. and Kimmel, G., Graded Al–AlN, TiN, and TiAlN multilayers deposited by radio-frequency reactive magnetron sputtering. *Surf. Coat. Technol.*, 1999, **114**, 269–277.
31. Porte, F., Etude du système halogénures d'aluminium/bases azotées: caractérisation des combinaisons azotées lors de la synthèse du nitrure d'aluminium à partir de la réaction avec les amines. PhD Thesis, Université de Limoges, 1998.
32. Antsiferov, V. N., Gilyov, V. G. and Karmanov, V. I., IR-spectra and phases structure of sialons. *Vibr. Spectrosc.*, 2002, **30**, 169–173.
33. Panneerselvam, M. and Rao, K. J., A microwave method for the preparation and sintering beta-SiAlON. *Mater. Res. Bull.*, 2003, **38**, 663–674.
34. Olivera, M., Olhero, S., Rocha, J. and Ferreira, J. M. F., Controlling hydrolysis and dispersion of AlN powders in aqueous media. *J. Coll. Interf. Sci.*, 2003, **261**, 456–463.
35. Hobert, H. and Dunken, H. H., Meinschien, Infrared and Raman spectroscopic investigation of thin films of AlN and SiC on Si substrates. *J. Stafast, H., Vibr. Spectrosc.*, 1999, **19**, 205–211.
36. Jimenez, C., Gilles, S., Doppelt, P., Bernard, C. and Madar, R., Preparation of aluminum nitride films by low pressure organometallic chemical vapor deposition. *Surf. Coat. Technol.*, 1995, **76/77**, 372–376.
37. Dimitrova, V., Manova, D., Paskova, T., Uzunov, Tz., Ivanov, N. and Dechev, D., Aluminum nitride thin films deposited by DC reactive magnetron sputtering. *Vaccum*, 1998, **51**(2), 161–164.
38. Dimitrova, V., Manova, D. and Djulgerova, R., Element composition and electrochemical behaviour of polycrystalline AlN thin films. *Surf. Coat. Technol.*, 2000, **123**, 12–16.
39. Tolle, J., Roucka, R., Chizmeshya, A. V. G., Crozier, P. A., Smith, D. J., Tsong, I. S. T. *et al.*, Novel synthetic pathways to wide bandgap semiconductors in the Si–C–Al–N system. *J. Sol. State Sci.*, 2002, **4**, 1509–1519.
40. Li, Y. Q., Qiu, T. and Xu, J., Effect of thermal oxidation treatment in air on the hydrolysis of AlN powder. *Mater. Res. Bull.*, 1997, **32**, 1173–1179.
41. Doucey, B., Nanocomposites Si_3N_4/SiC: stabilité thermique et densification de poudres SiCN(Al,O) synthétisées par pyrolyse laser—comportement au fluage des frittés. PhD Thesis, Université de Limoges, 1999.
42. Bahloul-Hourlier, D., Doucey, B., Besson, J.-L. and Goursat, P., Thermal reactivity of silicon-based nanopowders. In *Nanostructured Silicon-based Powders and Composites*, ed. A. P. Legrand and C. Sénémaud, 2003, pp. 41–53, London.
43. Cauchetier, M., Musset, E., Luce, M., Herlin, N., Armand, X. and Mayne, M., Laser synthesis of nanosized powders. In *Nanostructured Silicon-based Powders and Composites*, ed. A. P. Legrand and C. Sénémaud, 2003, pp. 6–24, London.
44. Dez, R., Ténégal, F., Reynaud, C., Mayne, M., Armand, X. and Herlin-Boime, N., Laser synthesis of silicon nanopowders, structure and thermal stability. *J. Eur. Ceram. Soc.*, 2002, **22**(16), 2969–2979.
45. Legrand, A. P., d'Espinose de la Caillerie, J. B. and El Kortobi, Y., Chemical order studied by solid-state nuclear magnetic resonance. In *Nanostructured Silicon-based Powders and Composites*, ed. A. P. Legrand and C. Sénémaud, 2003, pp. 111–138, London.
46. Champion, E., Goursat, P., Besson, J. L., Madigou, V., Monthioux, M. and Lespade, P., Microstructure, strength, and toughness of Si3N4-SiC whisker composites. In *Proceedings of the 16th Annual Conference on Composites and Advanced Ceramic Materials*, ed. J. B. Watchman, 1992.
47. Verdecia, G., O'Brien, K. L., Schmidt, W. R. and Apple, T. M., Aluminum-27 and silicon-29 solid-state nuclear magnetic resonance study of silicon carbide/aluminum nitride systems: effect of silicon/aluminum ratio and pyrolysis temperature. *Chem. Mater.*, 1998, **10**, 1003–1009.
48. McMillan, P. F., Sato, R. K. and Poe, B. T., Structural characterization of Si-Al-O-N glasses. *J. Non Cryst. Sol.*, 1998, **224**, 267–276.
49. Bräuniger, T., Kempgens, P., Harris, R. K., Howes, A. P., Liddell, K. and Thompson, D. P., A combined 14N/27Al nuclear magnetic resonance and powder X-ray diffraction study of impurity phasesin beta-sialon ceramics. *Sol. State Nucl. Magn. Reson.*, 2003, **23**, 62–76.
50. Birot, M., Pillot, J.-P. and Dunoguès, J., Comprehensive chemistry of polycarbosilanes, polysilazanes, and polycarbosilazanes as precursors of ceramics. *Chem. Rev.*, 1995, **95**, 1443–1477.
51. He, X.-M., Shu, L., Li, W.-Z. and Li, H.-D., Structure and properties of carbon nitride films synthesized by low energy ion bombardment. *J. Mater. Res.*, 1997, **12**(6), 1595–1602.
52. Wei, A., Chen, D., Ke, N., Peng, S. and Wong, S. P., Characteristics of carbon nitride films prepared by magnetic filtered plasma stream. *Thin Solid Films*, 1998, **323**, 217–221.
53. Jelínek, M., Zemek, J., Trchová, M., Vorlíček, V., Lančok, J., Tomov, R. *et al.*, CNx films created by combined laser deposition and r.f. discharge: XPS, FT-IR and Raman analysis. *Thin Solid Films*, 2000, **366**, 69–76.